Borneol-modified chitosan: Antimicrobial adhesion properties and application in skin flora protection

Yu Xin[a,b], Hongjuan Zhao[b], Jiangqi Xu[a], Zixu Xie[b], Guofeng Li[b], Zhihua Gan[b], Xing Wang[a,b,*]

[a] *Beijing Laboratory of Biomedical Materials, Beijing University of Chemical Technology, Beijing, 100029, PR China*
[b] *College of Life Science and Technology, Beijing University of Chemical Technology, Beijing, 100029, PR China*

ABSTRACT

Antimicrobial modifications of chitosan usually endow the products with strong bactericidal activities. However, if the products come into direct contact with human skin, the skin flora, which is beneficial to human health, may be damaged. To address this issue, we developed a stereochemical antimicrobial strategy by grafting borneol 4-formylbenzoate to chitosan using a stable Schiff base bond; this process yielded borneol-modified chitosan (BMC) as a novel antimicrobial material. This material was challenged with gram-negative *Escherichia coli*, gram-positive *Bacillus subtilis*, and *Aspergillus niger*. All tests showed excellent antimicrobial adhesive properties. Guinea pig skin experiments further demonstrated that BMC did not damage the skin flora. Owing to the antimicrobial mechanism of borneol stereochemistry, BMC successfully defended against pathogens and protected the skin flora. Thus, this material may have excellent potential applications in multifunctional textiles, healthcare, and flexible skin electronics.

1. Introduction

Chitosan, derived from the deacetylation of chitin (Hamed, Özogul, & Regenstein, 2016; Younes & Rinaudo, 2015; Zou et al., 2016) and the only pseudonatural cationic polymer (Bano, Arshad, Yasin, Ghauri, & Younus, 2017), is a well-known biomaterial with broad-spectrum antibacterial property (Jeon, Ma, Kang, Galvao, & Jeong, 2016; Ma et al., 2016; Su et al., 2017; Verlee, Mincke, & Stevens, 2017), good biocompatibility (Chen, Cheng et al., 2018; Zou et al., 2018), and high safety (Ali & Ahmed, 2018; Zargar, Asghari, & Dashti, 2015). Thus, chitosan is widely used in pharmaceutical (Fu et al., 2017; Shariatinia, 2018), food (Klein et al., 2016), cosmetics (Chen, Guo, & Luo, 2017), and textile industries (Kadam & Lee, 2015). However, studies have found that chitosan shows poor water solubility, displays good antibacterial activity in acidic aqueous solution (Zhao et al., 2017), and exhibits a steep decrease in antibacterial property after film formation (Foster & Butt, 2011; Torlak & Sert, 2013), which limits the broad application of chitosan. Therefore, some studies have proposed the establishment of new chitosan derivatives to improve solubility (Chen et al., 2016). Moreover, many modified chitosan derivatives have been developed to enhance the antibacterial properties of chitosan after film formation; in particular, researchers have examined the effects of

introduction of silver (Annur, Wang, Liao, & Kuo, 2015; Pinto et al., 2012; Raghavendra, Jung, & Seo, 2016), quaternary ammonium salt (Li et al., 2018; Vallapa et al., 2011), and antibacterial peptides (Costa, Carvalho, Montelaro, Gomes, & Martins, 2011) to chitosan. However, most of these modifications resulted in killing of microbes. In addition to providing protection against external infections, some microbes, such as those found in the skin flora, may be involved in host defense. The killing of the skin flora reduces the resistance of the host to pathogenic flora. Recently, Vandegrift et al. (2017) proposed a new hygienic concept to reduce the spread or transmission of pathogenic microorganisms. Therefore, it is necessary to develop new antimicrobial strategies involving chitosan derivatives to resist invasion of external pathogenic bacteria without harming the skin flora.

Our previous studies demonstrated that cells have different preferences for different chiral interfaces (Wang et al., 2010). Accordingly, we employed borneol, which has many chiral carbon atoms, to achieve antimicrobial adhesion by chiral stereochemistry. Borneol is a known natural antibiotic (Wang, Jing, Liu, Liu, & Tan, 2017) that is present in medicinal plants, such as lavender, alfalfa, and chamomile (Zhou, Zhang, Zhou, Fang, & Ge, 2016), and shows good antibacterial and anti-inflammatory effects. Borneol has four configurations, corresponding to different positions of the hydroxyl group (Luo et al., 2014). Researchers

Step 1:

Step 2:

Scheme 1. Synthesis of BF and subsequently grafting to CF/GC to obtain the BMC via an imidization method.

have found that L-borneol-based polymers exhibit good antimicrobial adhesion and biocompatibility and that the chirality of L-borneol is not affected after the general synthesis process (Li et al., 2017; Luo et al., 2014; Shi et al., 2015; Sun et al., 2016; Xu et al., 2018). Qian's group (Sun et al., 2016) also demonstrated the antimicrobial capacities of borneol-based copolymers. Based on these studies, we considered introducing L-borneol into chitosan to design a new type of antimicrobial chitosan. This method could endow the material with higher biological safety, particularly for the skin flora, and could show outstanding antimicrobial performance.

Accordingly, in this study, we used both chitosan fabric (CF) and glycol chitosan (GC) to evaluate antimicrobial effects. Commercial nonwoven CF is suitable for sample preparation and safety testing of skin flora, whereas GC has better solubility and film formation, making it more suitable for assaying antibacterial properties. L-Borneol was grafted to the CF/GC backbone by a two-step reaction (Scheme 1) to obtain borneol-modified chitosan (BMC). Borneol 4-formylbenzoate (BF) is a synthetic product derived from the esterification of 4-formylbenzoic acid with L-borneol to give an aldehyde group, which could react with the amino group of chitosan. The aldehyde group of BF reacted with the amino group of CF/GC to form Schiff base bonds, thus yielding the BMC. Both bacteria (gram-negative *Escherichia coli* (*E. coli*) and gram-positive *Bacillus subtilis* (*B. subtilis*)) and fungi (*Aspergillus niger* (*A. niger*)) were used to challenge the BMC. Finally, guinea pig skin experiments were performed to demonstrate the safety of the BMC with regard to the skin flora.

2. Experimental

2.1. Reagents and materials

GC (Wako; powder, molecular weight = 410 kDa, assay: 78.2%, degree of deacetylation: 85%), 4-formylbenzoic acid (J&K; 99%), L-borneol (J&K; 99%), *N,N*-dicyclohexyl carbodiimide (DCC; SCR; 95%), 4-dimethylaminopyridine (DMAP; TCI; 99%), 3-(4,5-dimethylazolyl-2)-2,5-diphenyltetrazolium bromide (MTT; TCI), 2,4-dinitrochlorobenzen (DNCB; Acros, China; 99%), silver nanoparticles (AgNPs; Stremchemical; 10 nm, 0.02 mg/mL in 2 mm sodium citrate), and CF (Hismer; spunlaced nonwoven, 50/50HS/HSX, degree of deacetylation: 93%) were used as received. Tetrahydrofuran (THF; J&K; 99.9%) was used after a dehydration treatment with molecular sieves. *B. subtilis* (ATCC 9372), *E. coli* (ATCC 25922), and *A. niger* (CICC 41254) were obtained from China Center of Industrial Culture Collection. Mouse fibroblasts (L929 cells) were purchased from Cell Resource Center, IBMS, CAMS/PUMC (Beijing, China). Roswell Park Memorial Institute (RPMI) 1640 medium, fetal bovine serum (FBS), and penicillin and streptomycin were purchased from Gibco BRL (Gaithersberg, MD, USA).

2.2. Synthesis and characterization of BF

4-Formylbenzoic acid (1.45 g, 9.66 mmol) was dissolved in 30 mL THF in round-bottomed flasks. DMAP (0.15 g, 1.2 mmol), DCC (2.60 g, 12.6 mmol), and L-borneol (1.00 g, 6.5 mmol) were added to the above solution, and the reaction was stirred at room temperature for 12 h. After suction filtration and rotary evaporation, the obtained pale yellow oily liquid was separated by silica gel column chromatography (200–300 mesh; the eluent was petroleum ether:ethyl acetate = 10:1). Finally, the white solid BF was obtained at a yield of 80%. Fourier transform infrared spectroscopy (FT-IR; IRAffinity-1; Shimadzu) and ^{1}H nuclear magnetic resonance (^{1}H NMR; DMSO; JNM-ECA400; JEOL) were used to confirm the chemical features of BF.

2.3. Preparation and characterization of BMC

For preparation of BMC samples for general characterization, 0.03 g GC was dissolved in 3 mL deionized water in a vial and kept at −20 °C overnight. Subsequently, the frozen samples were lyophilized (freeze dryer, −50 °C, 20 Pa; FD-1C-50; Boyikang Experimental Instrument Co., Ltd., Beijing, China) for 24 h. Next, 3 mL BF solution (1 wt% in ethanol) was added to the vial to immerse the as-prepared GC sponge for 12 h. After removing the unreacted BF ethanol solution, the sponge was washed with ethanol three times and then dried under vacuum conditions for 12 h. The aldehyde group of BF reacted with the amino group of GC to form a Schiff base bond, and finally, a borneol-modified GC sponge (BMGC) was obtained. The preparation of BMC on the CF substrate was carried out with the same procedure except for the frozen treatment. The CF was soaked in ethanol to wash out the impurities and air dried. The treated CF was immersed in BF solution (1 wt% in ethanol) overnight, and the borneol-modified CF (BMCF) material was then obtained after being rinsed with ethanol and air dried. The same treatment was applied to the CF substrate using 4-formylbenzoic acid (1 wt% in ethanol) to obtain 4-formylbenzoic acid-modified CF (FMCF) as a control.

FT-IR and ^{13}C NMR (solid state; AV300; Bruker) were performed to verify the structure of BMGC. Water contact angle (CA) measurements were performed at room temperature on a JC2000D3 (Zhongyi Kexin Technology Co., Ltd., Beijing, China) to detect the wettability of the CF, BMCF, GC, and BMGC samples. Energy dispersive spectroscopy (EDS; JSM-7800 F; JEOL) mapping was used to study the distributions of C, N, and O elements. Attenuated total reflection FT-IR (ATR-FTIR; Perkin-Elmer Spectrum 100 spectrometer; Waltham, MA, USA) was used to

observe the surface chemical structure of FMCF.

2.4. Antibacterial adhesion experiments

In order to evaluate the antibacterial adhesion activity of the BMC, a "prison break" experiment (Luo et al., 2014) was carried out by employing two typical bacteria: gram-positive *B. subtilis* and gram-negative *E. coli*. Briefly, polyethylene terephthalate (PET) plastics were cut into circular rings (inner diameter: 6 mm; outer diameter: 10 mm). The circular rings were immersed in GC solution (1 wt% in deionized water) for 6 h. After removing GC solution, the dried rings were soaked in BF solution (1 wt% in ethanol) for another 6 h. The above steps were repeated three times. Finally, BMGC materials with three layers were coated on the PET surface. GC was coated with the same method.

After being sterilized under ultraviolet light for 30 min per side, the PET (control), GC, and BMGC rings were immobilized on beef extract peptone medium, prepared by dissolving beef extract (3 g), peptone (10 g), sodium chloride (5 g), and agar (2 g) in deionized water (1000 mL, pH 7.0). Next, 1 μL of each bacterial suspension (10^6 CFU/mL) was added into the center of the three rings, and the rings were then incubated in a humidified incubator at 37 °C. At predetermined time intervals (0, 2, 4, and 5 days), the results of bacterial growth across the ring were recorded with a camera. The antibacterial adhesion experiments were carried out in triplicate.

2.5. Antifungal adhesion assay

In order to evaluate the antifungal activity of the BMC, a "landing test" experiment (Li et al., 2017) was carried out by employing *A. niger*. BMCF material was obtained according to the above method, and CF was used as a control. After sterilizing with ultraviolet light, the BMCF and CF materials were fixed onto the malt extract medium. Twenty microliters of *A. niger* suspension was added into the center of the plate, equidistant to the BMCF and CF disks. The solid medium was placed in a fungal incubator and aerobically cultured at 30 °C. Fungal growth was recorded using a camera at 0, 3, 10, 20, and 29 days, respectively.

After 29 days, the attachment of *A. niger* on the surface of the material was observed under higher magnification and photographed with an electronic camera. The BMCF and CF materials removed from malt extract medium were fixed with 2.5% glutaraldehyde, and soaked in a mixed solution of ethanol and isoamyl acetate with different concentrations. The number and morphology of *A. niger* adhered to the surface of the materials were observed by scanning electron microscopy (SEM; JSM-7800 F; JEOL).

In addition, in order to further explain the role of L-borneol in modulating the antibacterial properties of BMC materials, the control material FMCF was tested under the same conditions.

2.6. Skin flora evaluation

CF was cut into $2 \times 2\,cm^2$ pieces and modified as described above to obtain BMCF. CF pieces were then soaked in 1 mL AgNPs solution for 4 h at 4 °C, after drying under a vacuum; the obtained material was named CF-Ag and was used as a control group. After UV sterilization for 30 min, the BMCF and CF-Ag materials were used for evaluation of skin flora.

Twenty healthy albio guinea pigs (250–300 g, 10 males and 10 females), purchased from Beijing Vital River Experimental Animal Technique Ltd. Co. (license no. SCXK [Jing] 2011–0011), were treated and cared for in accordance with the National Research Council's Guide for the Care and Use of Laboratory Animals. Animals were shaved in a $3 \times 3\,cm^2$ area on both sides to ensure that the materials were in contact with the skin. The method for collecting skin microorganisms was performed as described by Williamson (1968). First, a cotton swab moistened with sterile physiological saline was used to wipe the designated area. Then, the prepared BMCF and CF-Ag materials were

attached to the shaved areas. After 6 h, the materials were removed, and the skin microorganisms were collected in the specific areas in the same manner. The cotton swab with skin microbes was placed in 3 mL saline and subjected to ultrasound vibration (ultrasonic cleaner, 40 kHz; KQ3200DE; Kunshan Shumei Ultrasonic Instrument Co., Ltd.) for 5 min. Next, 100 μL of the bacterium suspension was removed and cultured on TSA medium for 24 h. The results were recorded using a camera.

2.7. Skin sensitization test

Using the Buehler test (Buehler, 1965), skin sensitization of BMC was evaluated. The BMCF materials were obtained as described above. Briefly, 0.1 mL of 1 wt% DNCB was adsorbed on CF (CF-DNCB) as a positive control group, and a CF sample was used as a negative control group. The guinea pigs used in the experiment were similar to those described above. Guinea pigs were shaved on both sides of their bodies to form a $3 \times 3\,cm^2$ exposed area to facilitate material contact with the skin. BMCF, CF, and CF-DCNB ($2 \times 2\,cm^2$) were applied to the exposed area of the skin and removed after 6 h. Skin sensitization before and after material placement was recorded using a camera. This experiment was repeated three times.

2.8. In vitro biocompatibility evaluation

The biocompatibility of the tested materials was investigated with L929 cells. After adding 10% FBS, 100 units/mL penicillin, and 100 μg/mL streptomycin to RPMI-1640 medium, the obtained solution was used as a complete cell culture medium. L929 fibroblasts were cultured in the complete cell culture medium at 37 °C in a humidified environment of 95% air and 5% CO_2. The prepared BMGC and GC control were immersed in RPMI-1640 medium (2 mL) for 24 h, and the obtained leaching solution was then incubated with L929 cells in a 96-well plate. After 48 h of incubation, cell viability was determined using MTT colorimetric assays. An MTT colorimetric assay is known as a general method used to evaluate cell proliferation and cell viability. The relative growth rate (RGR) of the cells was calculated according to the following formula: RGR (%) = $Abs_{490sample}$ / $Abs_{490control}$ × 100, where $Abs_{490sample}$ and $Abs_{490control}$ are the absorbance of the samples and the reference at 490 nm, respectively.

3. Results and discussion

3.1. Synthesis and characterization of BF

FT-IR (Fig. S1) of BF showed an obvious absorption band at 1725 cm^{-1} attributed to the stretch vibration of −C═O. The asymmetric tensile vibration of the C−O−C of the linking group owing to the esterification reaction was found at 1276 cm^{-1} and 1108 cm^{-1}. Moreover, the −OH absorption peak of the borneol at 3300 cm^{-1} disappeared. These changes in the FT-IR spectrum demonstrated the successful synthesis of BF.

The chemical shift of the aldehyde at δ 10.13 ppm was clearly observed in the ^{1}H NMR of BF (Fig. S2). Additionally, the chemical shift of the benzene ring appeared at δ 8.08 and δ 8.16 ppm. The peaks of the cage structure of the borneol were also found at δ 0.8–0.9 and δ 1.0–2.3 ppm. The result of the ^{1}H NMR demonstrated that BF was synthesized successfully.

3.2. Synthesis and characterization of BMC

As shown in Scheme 1, BF was obtained via an esterification reaction. Subsequently, the aldehyde group of BF reacted with the amino group on the CF/GC surface to generate the Schiff base band of the BMC. Because of modification of the single layer of BF molecules, the BMCF maintained the same appearance. The enlarged SEM images (Fig. 1a and b) also did not show any differences in the fibrous
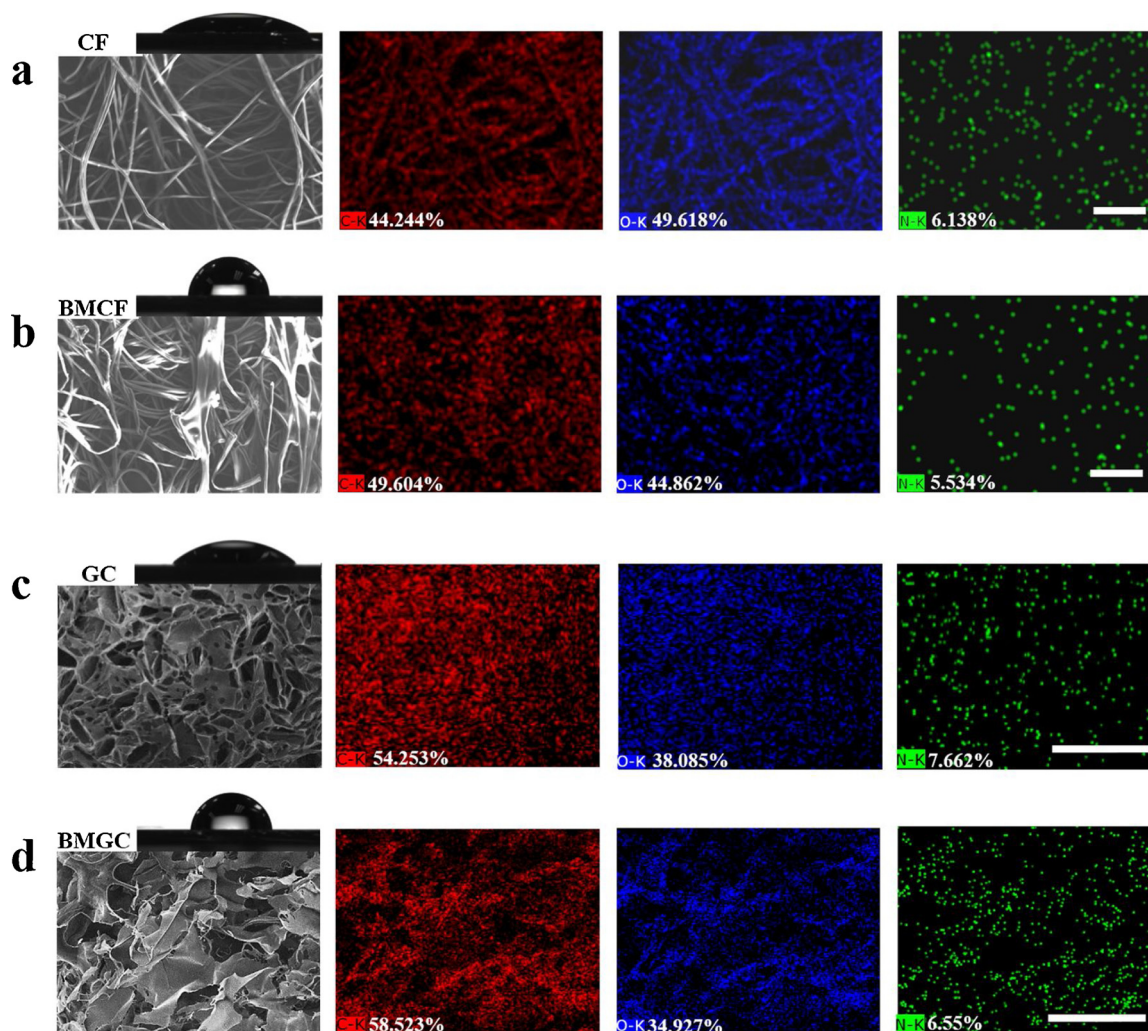
Fig. 1. SEM images of (a) CF, (b) BMCF, (c) GC, and (d) BMGC and the corresponding EDS mapping of C (red), O (blue), and N (green) elements. The scale bar is 300 μm. The inset shows the corresponding CA measurement. (For interpretation of the references to colour in this figure legend, the reader is referred to the web version of this article).

morphology. This modification was then evaluated by CA analysis. Compared with the CF substrate, which had a hydrophilic water CA of 27° (Fig. 1a), the BMCF surface exhibited more hydrophobic properties, with a water CA of 84° (Fig. 1b), indicating modification of hydrophobic BF molecules on the CF surface. EDS mapping was performed to determine the distribution of elements in the BMCF and CF samples (Fig. 1a and b). Compared with CF, the content of C increased in the BMCF sample, whereas the contents of N and O decreased somewhat. According to changes in N levels in EDS mapping, the grafting rate of BF was about 9.84% in BMCF. The uniform distribution of C and N also confirmed the homogeneous grafting of BF in the BMCF sample.

SEM imaging showed that the GC sponge exhibited a loose porous structure (Fig. 1c), which allowed BF to be in full contact with the sponge. Additionally, the BMGC sponge retained the same structure (Fig. 1d). The hydrophobicity of the BMGC sponge was significantly increased (water CA: 85°) compared with that of the GC sponge (water CA: 35°; Fig. 1c, d), indicating that the hydrophobic BF was grafted onto the GC sponge. Similarly, the element distributions of GC and BMGC were characterized by EDS mapping (Fig. 1c and d). Owing to differences in chitosan contents of GC and CF, their elemental distributions were slightly different, although changes in the elemental compositions of the materials after grafting BF were similar. The content of C in the BMGC samples increased, whereas the contents of N and O decreased. The decrease in N content shown by EDS mapping demonstrated that

the graft ratio of BF on the BMGC material was approximately 14.51%.

The synthesized Schiff base in the BMGC was characterized by combining measurements of FT-IR and NMR. The typical spectra of BMGC and GC are shown in Fig. 2a. A significant peak at 1640 cm^{-1} was detected in the BMGC sample, corresponding to the C=N stretching of the Schiff base bond, indicating that BF was grafted onto the GC. Subsequently, an obvious vibration peak at 1720 cm^{-1}, which corresponded to the C=O vibration of the ester bond, was observed in the spectral characteristics of BMGC. Simultaneously, vibration of the C−O−C of the linking group produced by the esterification reaction was found at 1275 cm^{-1}. Consequently, an increased vibration peak at 2876 cm^{-1}, which corresponded to the C−H stretching of methyl or methylene, was observed in the spectral characteristics of BMGC. Furthermore, in the BMGC spectrum rather than the GC spectrum, a distinct signal peak was observed at 770 cm^{-1} due to the stretching vibration of C−H in the benzene ring, and the carbon skeleton stretching vibration of the benzene ring also appeared at 1456 cm^{-1}. Because of the presence of glucose units, both the GC and BMGC spectra had significant O−H stretching vibrations (3200–3600 cm^{-1}), C−H stretching vibrations (2928 cm^{-1}), and C−O stretching vibrations (1052 cm^{-1}). These findings confirmed the successful grafting of BF in BMGC samples.

Further evidence of BMGC product synthesis was provided by ^{13}C NMR. The results of ^{13}C NMR analysis of BMGC, BF, and GC groups are

a

b
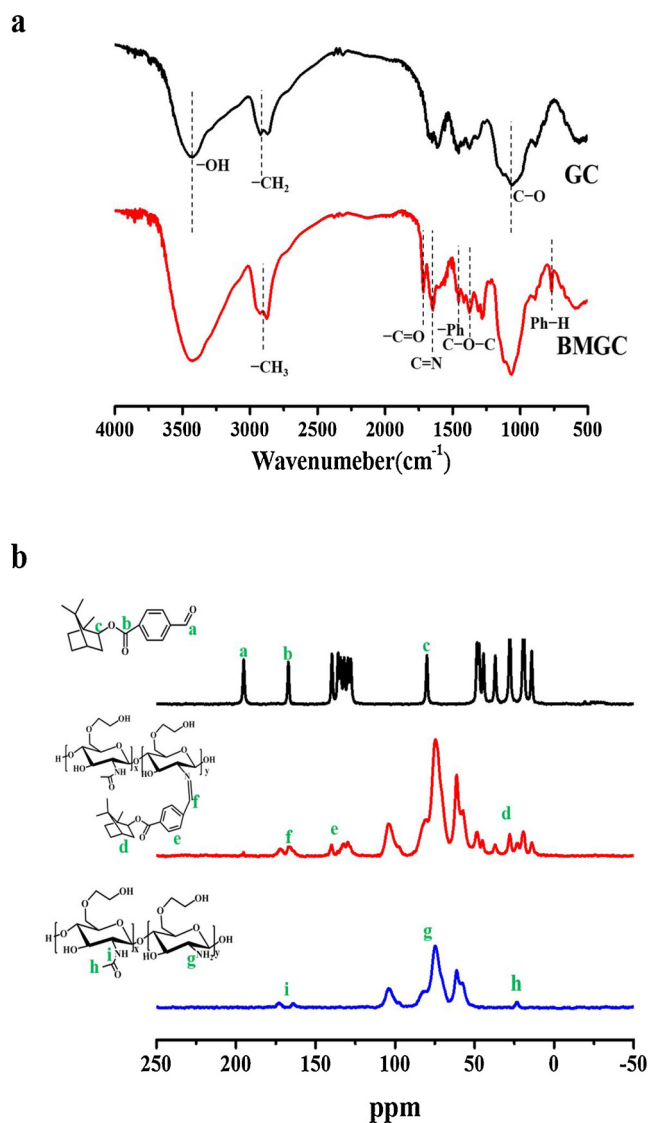
Fig. 2. (a) FT-IR of GC and BMGC. (b) ^{13}C NMR of BF (top), BMGC (middle), and GC (bottom).

shown in Fig. 2. Compared with GC, the BMGC spectrum showed two prominent signal peaks at δ 10–50 ppm (bond d) and δ 130–140 ppm (bond e), representing the benzene ring and cage structures on the grafted BF. Furthermore, in the BMGC spectrum, the signal peak of the aldehyde group at δ 195 ppm (bond a) disappeared owing to the reaction of the aldehyde group of BF with the amino group of GC. The peak of the Schiff base bond formed by the reaction was δ 166 ppm (bond f), which overlapped with the position of the acetyl peak at δ 164 ppm (bond i) in the GC spectrum. The ^{13}C nucleus properly illustrates the structure of the BMGC.

To illustrate the grafting of 4-formylbenzoic acid on CF, ATR-FTIR spectroscopy was performed on FMCF (Fig. S3). A broad absorption peak appeared in the spectrum of FMCF at 3100–3500 cm^{-1}, corresponding to the O−H absorption of the carboxyl group on the grafted 4-formylbenzoic acid. Then, the peak of carboxyl O−H was also found at 891 cm^{-1}. Moreover, a distinct new absorption peak appeared at 670 cm^{-1} of the FMCF spectrum, which was caused by vibration of the C−H bond on the benzene ring. ATR-FTIR indicated that the synthesis of the control material FMCF was successful.

3.3. Antibacterial adhesion capability

A bacterial "prison break" experiment (Fig. 3a) was used to evaluate the antibacterial adhesion capacity of the BMC material. In this experiment, raw PET and the GC coating rings were used as control groups (the GC coating ring was more suitable than the CF ring owing to the roughness and porosity of the CF ring). Fig. 3b shows the challenge with gram-negative *E. coli* for evaluating the test rings. On the second day of culture, *E. coli* was found to have grown beyond the PET ring, indicating that this material was not antibacterial. However, *E. coli* was still limited by the GC and BMGC rings. Indeed, previous reports have shown that GC has bactericidal effects (Biao et al., 2017); however, this ability was not strong on the sample surface because the surviving bacteria grew outside of the GC ring by day 4. In contrast, the BMGC ring blocked the growth of *E. coli* until day 5. Thus, BMGC had good capacity for inhibiting the expansion of *E. coli*. Compared with GC, BMGC showed significantly enhanced antibacterial adhesion capability.

Moreover, gram-positive *B. subtilis* was employed to test the BMGC material in order to further evaluate its broad antibacterial adhesion properties (Fig. 3c). In contrast to the experiment with *E. coli*, the GC ring was first broken on day 2 of culture. We speculate that GC may have good water solubility, resulting in partially dissolution on the surface of the medium and permitting the bacteria located in the center of the ring to move outside of the ring. On day 4 of culture, *B. subtilis* broke through the PET and GC rings, but not the BMGC ring. The colony of *B. subtilis* around the PET ring was uniform and larger than that outside the GC ring. This phenomenon confirmed our findings that during the process of bacterial growth, GC exhibited weak bactericidal effect, but that this bactericidal effect was too limited to inhibit bacterial reproduction. Moreover, owing to partial dissolution of the GC on the medium, colonies outside the GC loop grew in a nonuniform direction. This performance was consistent with the results for *E. coli*. Additionally, until day 5, only a small amount of *B. subtilis* spread outside the BMGC ring, demonstrating that the BMGC material could inhibit bacterial adhesion, including both gram-positive and gram-negative bacteria, mainly because of the modification with L-borneol.

3.4. Antifungal adhesive assay

In studies of chitosan modification, the improvement of antibacterial and antifungal properties has been extensively studied (Sathiyabama & Parthasarathy, 2016; Verlee et al., 2017). In this study, *A. niger* was used as a test strain to evaluate the antifungal adhesion of the BMC using the "landing test" (Fig. 4). The BMCF and CF disks (d =6 mm) were placed on malt extract medium containing 20 μL of an *A. niger* suspension added to the center of the medium. After 3 days, *A. niger* spread to the edge of both the BMCF and CF disks. A significant difference was found, and this difference became more obvious after culture for 10 days. The CF disk was covered by *A. niger*, whereas the BMCF disk was very clean, even until 29 days of culture. Using an ordinary microscope, a high density of fungal cells was found to cover the surface of the CF disk. Conversely, the BMCF disk exhibited a clear surface without any *A. niger* spores adhering or growing on it, except for a few of dropped spores found at the edges. The fungal spores surrounded the disk, demonstrating the excellent antifungal adhesion performance of BMCF.

To examine whether the antibacterial adhesion of BMCF was based on the chiral effects introduced by L-borneol, we tested the antifungal adhesion of FMCF, as shown in Fig. S3. After 7 days of culture, both CF and FMCF materials were stained with *A. niger*. spore coverage, suggesting that FMCF had no anti-adhesion ability. Thus, we concluded that the antibacterial ability of BMCF was related to the grafting of L-borneol.

SEM measurements were carried out to study the microscopic adhesion of *A. niger* on the surface of the BMCF and CF disks (Fig. 5). Many *A. niger* cells adhered to the surface of the CF disk (Fig. 5a1). At
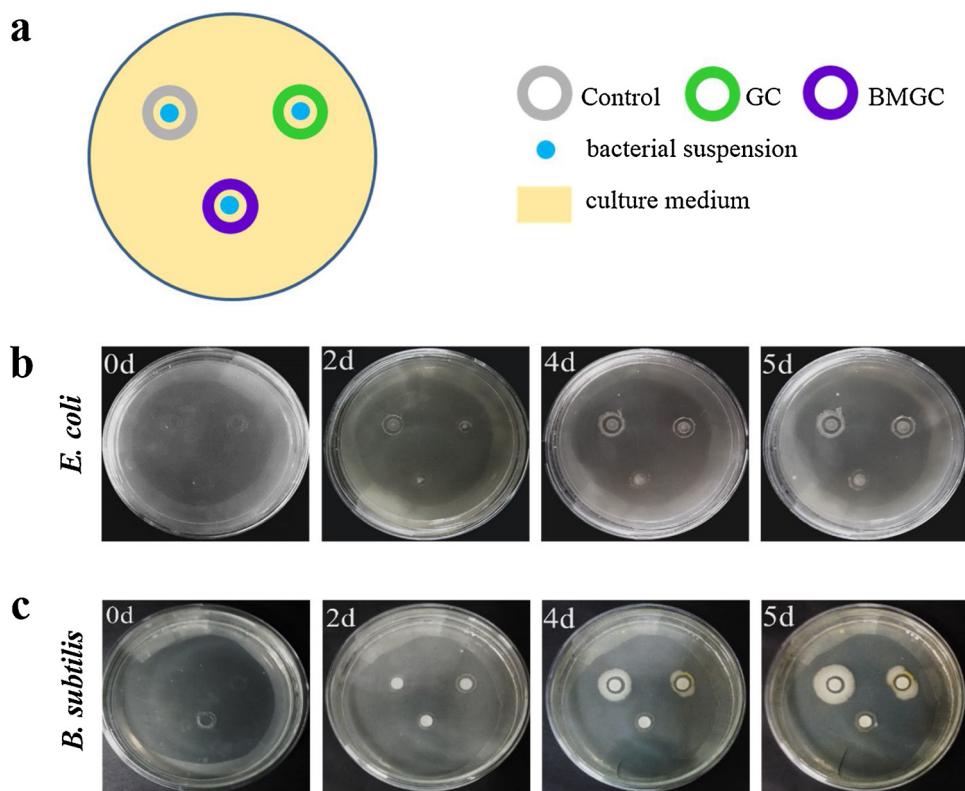
Fig. 3. (a) Schematic diagram of the "prison break" test for antibacterial adhesion evaluation. Effects on controlling the escape of gram-negative *E. coli* (b) and gram-positive *B. subtilis* (c) for the PET control, GC coating, and BMGC rings after different incubation times.
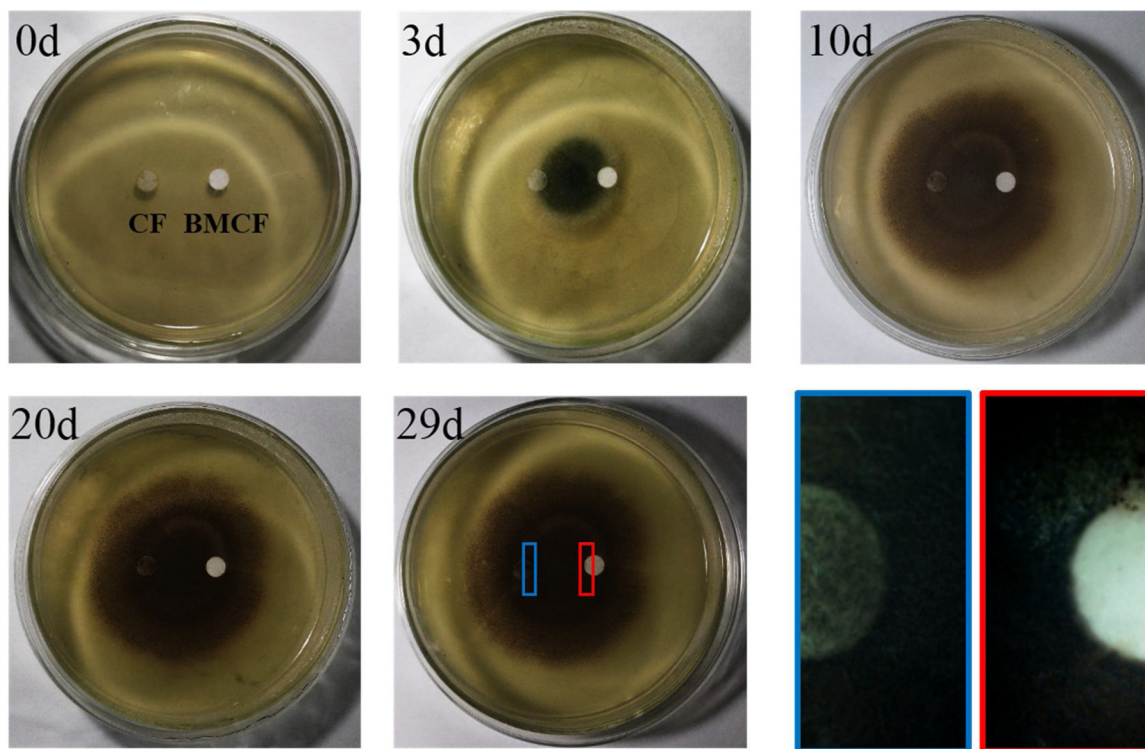
Fig. 4. Landing test for the effects of antifungal adhesion on the CF (left) and BMCF (right) disks, by culturing *A. niger* for 0, 3, 10, 20, and 29 days. Enlarged images of the red and blue boxes show the test results for the BMCF and CF disks, respectively. (For interpretation of the references to colour in this figure legend, the reader is referred to the web version of this article).
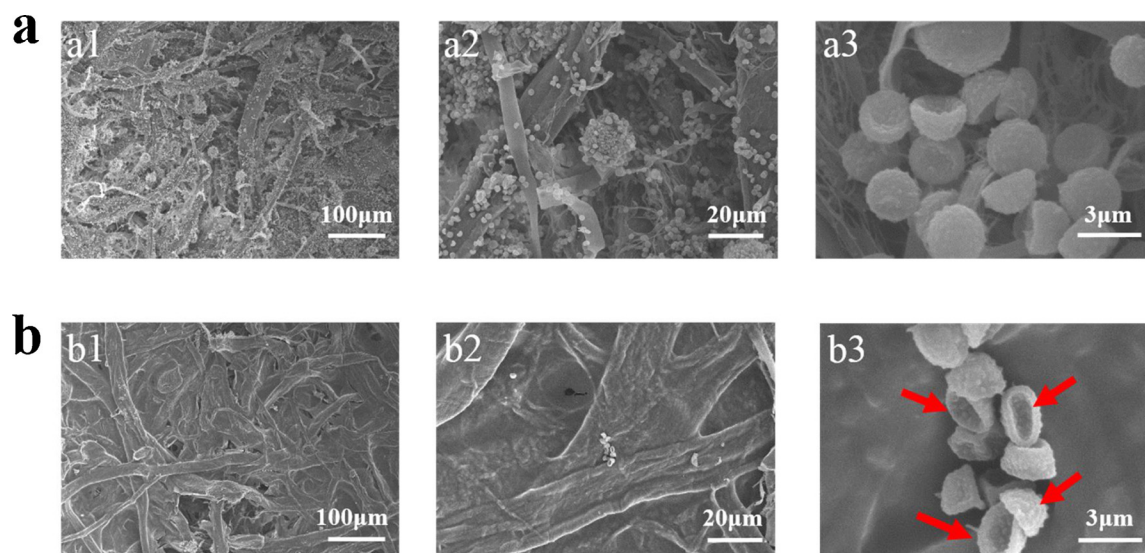
Fig. 5. SEM images of the antifungal adhesion results, (a) on the CF surface and (b) on the BMCF surface. Red arrows indicate depressions and shriveled structures of the spores. (For interpretation of the references to colour in this figure legend, the reader is referred to the web version of this article).
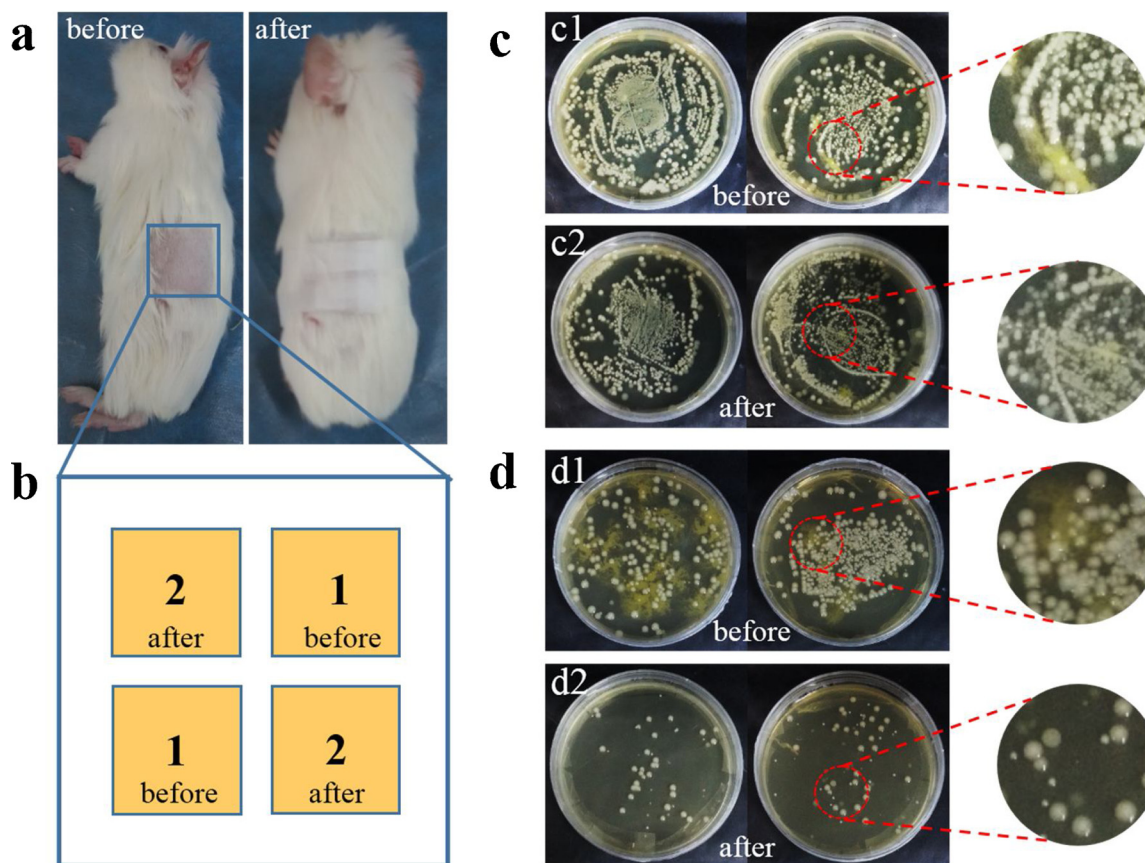
Fig. 6. (a) Animal model of the skin flora experiment. (b) The yellow region represents the shaved region of the guinea pig. Regions 1 and 2 are the locations of skin flora collection before and after the materials were applied, respectively. (c) Culture results of the skin flora before (c1) and after (c2) wearing the BMCF material. (d) Culture results of the skin flora before (d1) and after (d2) wearing the CF-Ag material. The illustration on the right is a partial enlargement of the culture results for c1, c2, d1, and d2. (For interpretation of the references to colour in this figure legend, the reader is referred to the web version of this article).

higher magnification (Fig. 5a2 and a3), *A. niger* attached to the CF surface grew very well, showing many sporangia and germinating spores. The CF material had no effect on preventing adhesion of fungal stains. Although many *A. niger* cells propagated on the culture medium, the BMCF material surface was still very clean (Fig. 5b1). Only a few scattered spores were observed at the edge of the BMCF disk (Fig. 5b2).

Moreover, the spores were obviously small and shriveled (Fig. 5b3, red arrow), demonstrating that the BMCF material was not conducive to the growth of *A. niger*. Thus, the grafting of ʟ-borneol conferred the BMCF material with excellent resistance to fungal adhesion.

Table 1
Sequence analysis of guinea pig skin strains.

Test strain	Species name from 16 s rDNA identification	Similarity rate	Gene bank (ID)
White bacteria	*Kurthia* sp.	99%	CP013217.1
Yellow flocculent	*Acinetobacter* sp.	99%	KC257007.1

3.5. Skin flora evaluation

Recent studies have shown that the skin flora is involved in host defense during the invasion of pathogenic bacteria (Chen, Fischbach, & Belkaid, 2018; Naik et al., 2012). Indeed, the skin flora plays an important role in the barrier function of skin. Once the skin flora is destroyed, the barrier function is also disrupted (Baldwin et al., 2017), potentially leading to infection by pathogenic bacteria. Accordingly, we assumed that antibacterial materials in contact with the skin should prevent bacteria from adhering to the surface of the material, thus resisting invasion and maintaining the balance of the skin flora, rather than killing the skin flora. Traditional antibacterial materials, such as metallic silver ions, have good antibacterial effects, but also threaten the skin flora. Therefore, we performed an experiment using guinea pig skin flora to investigate whether our newly developed materials caused damage to the skin flora.

Fig. 6a shows the animal model. The BMCF and CF-Ag materials were placed on the bare skin of the guinea pig and then removed after 6 h. According to the design (Fig. 6b), bacteria were collected from region 1 before the material was applied and from region 2 after the material was removed. The results are shown in Fig. 6c and d. Fig. 6c1 shows an abundance of yellow flocculent and white clustered microorganisms in the culture plate. Identification of bacteria using the 16 s rDNA method (Table 1) showed that the white bacteria belonged to *Acinetobacter* sp., which also exists on the surface of healthy human skin and can be classified as a symbiotic flora. The yellow flocculent belonged to *Kurdish* sp., which is often present in feces and can be classified as a cross-flora. After wearing the BMCF for 6 h, both the species and number of the detected microorganisms were not changed (Fig. 6c2, inset). However, after wearing the traditional bactericidal CF-Ag for 6 h, the number of microorganisms was obviously decreased (Fig. 6d, inset). The results suggested that the white *Acinetobacter* sp.
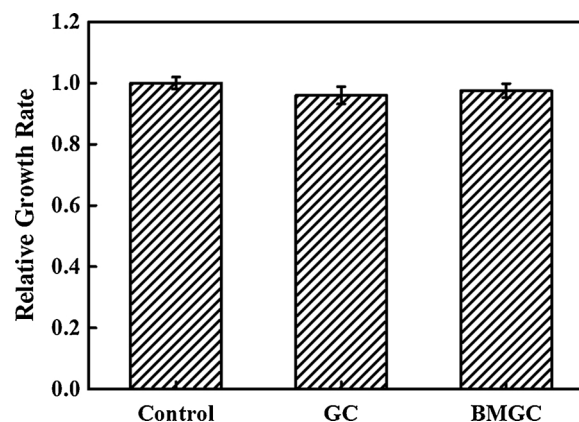
Fig. 8. MTT results of the RGR in L929 cells after 48 h of incubation with the corresponding GC and BMGC conditioned medium.

were mostly killed, though the yellow *Kurdish* sp. were also decreased. These phenomena were not the desired results for antimicrobial CF, because it caused damage to the skin flora. Therefore, compared with the bactericidal material, BMCF showed the ability to manage and control microbes, i.e., maintained the balance between antimicrobial properties and skin flora.

3.6. Skin sensitization test

A skin sensitization experiment using guinea pigs as a test model was then performed using Buehler tests. As shown in Fig. 7, after the BMCF was applied to the skin for 6 h, there was no erythema or edema on the surface of the guinea pig skin, consistent with the results for the negative control group. However, after contact of the positive control group (CF-DNCB) with the guinea skin, there was obvious erythema with slight swelling. Referring to the Magnusson and Kligman scale (ISO 10993.10-2010), the BMCF material had a sensitization level of 0, indicating that this material was nonsensitizing. This phenomenon suggested that the BMCF did not induce skin sensitization and could be safely used in the textile field.
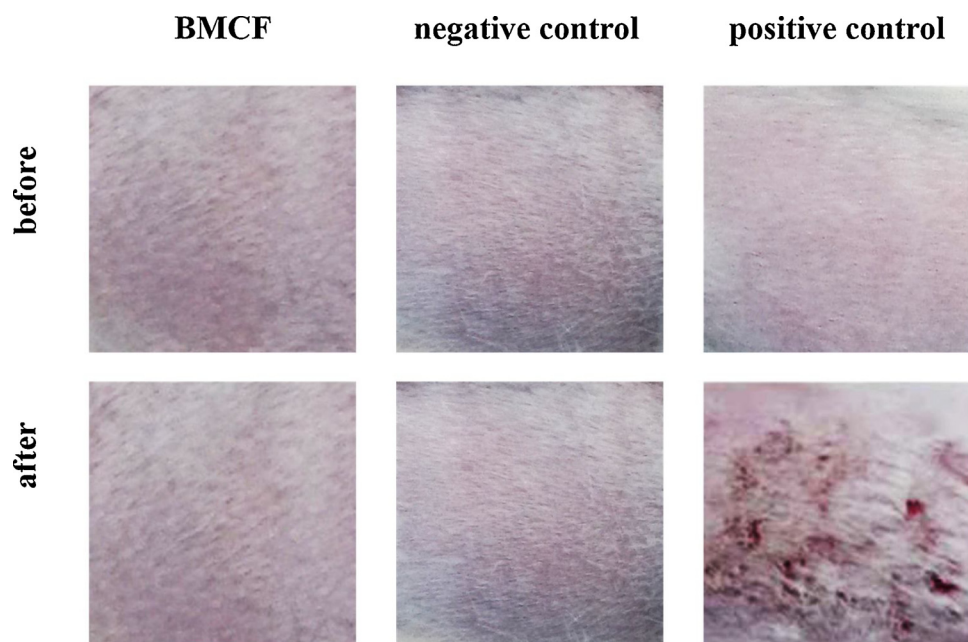
Fig. 7. Skin sensitization experiments for BMCF, CF (negative control), and CF-DNCB (positive control) before and after contact with guinea pig skin.

3.7. Biocompatibility

MTT experiments were used to evaluate material biocompatibility. Fig. 8 shows the RGR results in L929 cells for all test materials, including the BMGC sample. After 48 h of incubation, the viability of cells in contact with the BMGC material was 97.48% ± 2.30%, which was slightly higher than that of the GC material (95.99% ± 2.85%). According to the relationships between RGR and cytotoxicity in the Pharmacopoeia of United States (USP, Table S2), the toxicity of BMGC was grade 1. Based on the standard toxicity rating, grade 1 indicates no toxicity within the safety framework for use. Therefore, BMGC material was found to be nontoxic and had good biocompatibility.

4. Conclusion

In summary, we developed a novel BMC material that may effectively resist pathogens and protect the skin flora. BMC exhibited good antibacterial adhesion properties against both gram-positive and gram-negative bacteria. In addition, the BMC materials also displayed excellent antifungal adhesion performance for up to 29 days. Hence, BMC could be considered a broad-spectrum antimicrobial material. Further studies indicated that BMC did not cause damage to the skin flora and did not induce skin sensitization. Moreover, BMC enhanced the protective effects of CF with regard to the potential attachment of pathogens and maintained the skin flora. Therefore, BMC could have applications as a novel biomaterial based on the stereochemical antimicrobial strategy, effectively enhancing the antimicrobial properties of chitosan after direct modification or film formation. Stereochemical antimicrobial strategies are expected to lead to additional opportunities for managing and controlling microorganisms.

Acknowledgment

Appendix A. Supplementary data

Supplementary material related to this article can be found, in the online version, at doi:https://doi.org/10.1016/j.carbpol.2019.115378.

References

Ali, A., & Ahmed, S. (2018). A review on chitosan and its nanocomposites in drug delivery. *International Journal of Biological Macromolecules, 109*, 273–286.

Annur, D., Wang, Z. K., Liao, J. D., & Kuo, C. (2015). Plasma-synthesized silver nanoparticles on electrospun chitosan nanofiber surfaces for antibacterial applications. *Biomacromolecules, 16*(10), 3248–3255.

Baldwin, H. E., Bhatia, N. C., Friedman, A., Prunty, T., Martin, R., & Seite, S. (2017). The role of cutaneous microbiota harmony in maintaining a functional skin barrier. *SKIN the Journal of Cutaneous Medicine, 1*(3.1), s139.

Bano, I., Arshad, M., Yasin, T., Ghauri, M. A., & Younus, M. (2017). Chitosan: A potential biopolymer for wound management. *International Journal of Biological Macromolecules, 102*, 380–383.

Biao, L., Tan, S., Wang, Y., Guo, X., Fu, Y., Xu, F., & Liu, Z. (2017). Synthesis, characterization and antibacterial study on the chitosan-functionalized Ag nanoparticles. *Materials Science and Engineering C, 76*, 73–80.

Buehler, E. V. (1965). Delayed contact hypersensitivity in the guinea pig. *Archives of Dermatology, 91*(2), 171–175.

Chen, Y. E., Fischbach, M. A., & Belkaid, Y. (2018). Skin microbiota–host interactions. *Nature, 553*(7689), 427.

Chen, Y., Li, J., Li, Q., Shen, Y., Ge, Z., Zhang, W., & Chen, S. (2016). Enhanced water-solubility, antibacterial activity and biocompatibility upon introducing sulfobetaine and quaternary ammonium to chitosan. *Carbohydrate Polymers, 143*, 246–253.

Chen, K., Guo, B., & Luo, J. (2017). Quaternized carboxymethyl chitosan/organic montmorillonite nanocomposite as a novel cosmetic ingredient against skin aging. *Carbohydrate Polymers, 173*, 100–106.

Chen, J., Cheng, G., Liu, R., Zheng, J., Huang, M., Yi, Y., & Deng, H. (2018). Enhanced physical and biological properties of silk fibroin nanofibers by layer-by-layer deposition of chitosan and rectorite. *Journal of Colloid and Interface Science, 523*,

208–216.

Costa, F., Carvalho, I. F., Montelaro, R. C., Gomes, P., & Martins, M. C. L. (2011). Covalent immobilization of antimicrobial peptides (AMPs) onto biomaterial surfaces. *Acta Biomaterialia, 7*(4), 1431–1440.

Foster, L. J. R., & Butt, J. (2011). Chitosan films are NOT antimicrobial. *Biotechnology Letters, 33*(2), 417–421.

Fu, Y. N., Li, Y., Li, G., Yang, L., Yuan, Q., Tao, L., & Wang, X. (2017). Adaptive chitosan hollow microspheres as efficient drug carrier. *Biomacromolecules, 18*(7), 2195–2204.

Hamed, I., Özogul, F., & Regenstein, J. M. (2016). Industrial applications of crustacean by-products (chitin, chitosan, and chitooligosaccharides): A review. *Trends in Food Science & Technology, 48*, 40–50.

Jeon, S. J., Ma, Z., Kang, M., Galvao, K. N., & Jeong, K. C. (2016). Application of chitosan microspheres for treatment of metritis and in vivo evaluation of broad spectrum antimicrobial activity in cow uteri. *Biomaterials, 110*, 71–80.

Kadam, A. A., & Lee, D. S. (2015). Glutaraldehyde cross-linked magnetic chitosan nanocomposites: Reduction precipitation synthesis, characterization, and application for removal of hazardous textile dyes. *Bioresource Technology, 193*, 563–567.

Klein, M. P., Hackenhaar, C. R., Lorenzoni, A. S., Rodrigues, R. C., Costa, T. M., Ninow, J. L., & Hertz, P. F. (2016). Chitosan crosslinked with genipin as support matrix for application in food process: Support characterization and β-d-galactosidase immobilization. *Carbohydrate Polymers, 137*, 184–190.

Li, G., Zhao, H., Hong, J., Quan, K., Yuan, Q., & Wang, X. (2017). Antifungal graphene oxide-borneol composite. *Colloids and Surfaces B, Biointerfaces, 160*, 220–227.

Li, J., Xie, B., Xia, K., Zhao, C., Li, Y., Li, D., & Han, J. (2018). Facile synthesis and characterization of cross-linked chitosan quaternary ammonium salt membrane for antibacterial coating of piezoelectric sensors. *International Journal of Biological Macromolecules, 120*, 745–752.

Luo, L., Li, G., Luan, D., Yuan, Q., Wei, Y., & Wang, X. (2014). Antibacterial adhesion of borneol-based polymer via surface chiral stereochemistry. *ACS Applied Materials & Interfaces, 6*(21), 19371–19377.

Ma, Z., Kim, D., Adesogan, A. T., Ko, S., Galvao, K., & Jeong, K. C. (2016). Chitosan microparticles exert broad-spectrum antimicrobial activity against antibiotic-resistant micro-organisms without increasing resistance. *ACS Applied Materials & Interfaces, 8*(17), 10700–10709.

Naik, S., Bouladoux, N., Wilhelm, C., Molloy, M. J., Salcedo, R., Kastenmuller, W., ... Belkaid, Y. (2012). Compartmentalized control of skin immunity by resident commensals. *Science, 337*(6098), 1115–1119.

Pinto, R. J., Fernandes, S. C., Freire, C. S., Sadocco, P., Causio, J., Neto, C. P., & Trindade, T. (2012). Antibacterial activity of optically transparent nanocomposite films based on chitosan or its derivatives and silver nanoparticles. *Carbohydrate Research, 348*, 77–83.

Raghavendra, G. M., Jung, J., & Seo, J. (2016). Microwave assisted antibacterial chitosan–silver nanocomposite films. *International Journal of Biological Macromolecules, 84*, 281–288.

Sathiyabama, M., & Parthasarathy, R. (2016). Biological preparation of chitosan nanoparticles and its in vitro antifungal efficacy against some phytopathogenic fungi. *Carbohydrate Polymers, 151*, 321–325.

Shariatinia, Z. (2018). Pharmaceutical applications of chitosan. *Advances in Colloid and Interface Science*.

Shi, B., Luan, D., Wang, S., Zhao, L., Tao, L., Yuan, Q., & Wang, X. (2015). Borneol-grafted cellulose for antifungal adhesion and fungal growth inhibition. *RSC Advances, 5*(64), 51947–51952.

Su, Y., Tian, L., Yu, M., Gao, Q., Wang, D., Xi, Y., & Li, P. (2017). Cationic peptidopolysaccharides synthesized by 'click'chemistry with enhanced broad-spectrum antimicrobial activities. *Polymer Chemistry, 8*(25), 3788–3800.

Sun, X., Qian, Z., Luo, L., Yuan, Q., Guo, X., Tao, L., & Wang, X. (2016). Antibacterial adhesion of poly (methyl methacrylate) modified by borneol acrylate. *ACS Applied Materials & Interfaces, 8*(42), 28522–28528.

Torlak, E., & Sert, D. (2013). Antibacterial effectiveness of chitosan–propolis coated polypropylene films against foodborne pathogens. *International Journal of Biological Macromolecules, 60*, 52–55.

Vallapa, N., Wiarachai, O., Thongchul, N., Pan, J., Tangpasuthadol, V., Kiatkamjornwong, S., & Hoven, V. P. (2011). Enhancing antibacterial activity of chitosan surface by heterogeneous quaternization. *Carbohydrate Polymers, 83*(2), 868–875.

Vandegrift, R., Bateman, A. C., Siemens, K. N., Nguyen, M., Wilson, H. E., Green, J. L., ... Hickey, R. J. (2017). Cleanliness in context: Reconciling hygiene with a modern microbial perspective. *Microbiome, 5*(1), 76.

Verlee, A., Mincke, S., & Stevens, C. V. (2017). Recent developments in antibacterial and antifungal chitosan and its derivatives. *Carbohydrate Polymers, 164*, 268–283.

Wang, X., Gan, H., Sun, T., Su, B., Fuchs, H., Vestweber, D., & Butz, S. (2010). Stereochemistry triggered differential cell behaviours on chiral polymer surfaces. *Soft Matter, 6*(16), 3851–3855.

Wang, X., Jing, S., Liu, Y., Liu, S., & Tan, Y. (2017). Diblock copolymer containing bioinspired borneol and dopamine moieties: Synthesis and antibacterial coating applications. *Polymer, 116*, 314–323.

Williamson, P. (1968). A new method for the quantitative investigation of cutaneous propionibacteria. *The Journal of Investigative Dermatology, 45*, 498–503.

Xu, J., Bai, Y., Wan, M., Liu, Y., Tao, L., & Wang, X. (2018). Antifungal paper based on a polyborneolacrylate coating. *Polymers, 10*(4), 448.

Younes, I., & Rinaudo, M. (2015). Chitin and chitosan preparation from marine sources. Structure, properties and applications. *Marine Drugs, 13*(3), 1133–1174.

Zargar, V., Asghari, M., & Dashti, A. (2015). A review on chitin and chitosan polymers: Structure, chemistry, solubility, derivatives, and applications. *ChemBioEng Reviews, 2*(3), 204–226.

Zhao, X., Wu, H., Guo, B., Dong, R., Qiu, Y., & Ma, P. X. (2017). Antibacterial anti-oxidant electroactive injectable hydrogel as self-healing wound dressing with hemostasis and

adhesiveness for cutaneous wound healing. *Biomaterials, 122*, 34–47.

Zhou, H. H., Zhang, L., Zhou, Q. G., Fang, Y., & Ge, W. H. (2016). (+)-Borneol attenuates oxaliplatin-induced neuropathic hyperalgesia in mice. *NeuroReport, 27*(3), 160–165.

Zou, W., Chen, Y., Zhang, X., Li, J., Sun, L., Gui, Z., & Chen, S. (2018). Cytocompatible chitosan based multi-network hydrogels with antimicrobial, cell anti-adhesive and

mechanical properties. *Carbohydrate Polymers, 202*, 246–257.

Zou, P., Yang, X., Wang, J., Li, Y., Yu, H., Zhang, Y., & Liu, G. (2016). Advances in characterisation and biological activities of chitosan and chitosan oligosaccharides. *Food Chemistry, 190*, 1174–1181.